IOPscience iopscience.iop.org

Home Search Collections Journals About Contact us My IOPscience

Raman scattering in $La_{1-x}Sr_xFeO_{3-}$ thin films: annealing-induced reduction and phase transformation

This content has been downloaded from IOPscience. Please scroll down to see the full text.

2015 J. Phys.: Condens. Matter 27 155401

(http://iopscience.iop.org/0953-8984/27/15/155401)

View the table of contents for this issue, or go to the journal homepage for more

Download details:

IP Address: 144.118.116.19
This content was downloaded on 16/10/2015 at 15:45

Please note that terms and conditions apply.

IOP Publishing Journal of Physics: Condensed Matter
J. Phys.: Condens. Matter **27** (2015) 155401 (7pp) doi:10.1088/0953-8984/27/15/155401

Raman scattering in $La_{1-x}Sr_xFeO_{3-\delta}$ thin films: annealing-induced reduction and phase transformation

Mohammad A Islam, Yujun Xie, Mark D Scafetta, Steven J May and Jonathan E Spanier

Department of Materials Science and Engineering, and the A J Drexel Institute for Energy and the Environment, Drexel University, Philadelphia, PA 19104, USA

E-mail: spanier@drexel.edu

Received 12 August 2014, revised 5 January 2015
Accepted for publication 9 February 2015
Published 27 March 2015

Abstract

Raman scattering in thin film $La_{0.2}Sr_{0.8}FeO_{3-\delta}$ on MgO(0 0 1) collected at 300 K after different stages of annealing at selected temperatures T (300 K $< T <$ 543 K, to 10 h) and analysis reveal changes in spectral characteristics due to a loss of oxygen, onset of oxygen vacancy-induced disorder, and activation of Raman-inactive modes that are attributed to symmetry lowering. The interpretation is further supported by carrier transport measurements under identical conditions showing orders of magnitude increase in the resistivity induced by oxygen loss. After prolonged annealing in air, evolution of the spectrum signals the appearance of a possible topotactic transformation of the crystal structure from that of the rhombohedral ABO_3 perovskites to that of Brownmillerite-like structure consisting of octahedrally and tetrahedrally coordinated Fe atoms.

Keywords: complex oxide perovskite, Raman scattering, topotactic phase transformation

(Some figures may appear in colour only in the online journal)

1. Introduction

The ground state of many ABO_3 type perovskites is composed of several competing phases and the phase space is susceptible to many external stimuli, including electric field, temperature and the presence of reactive species [1]. A novel property of $ABO_{3-\delta}$ perovskites is the ability of these materials to accommodate oxygen vacancies in the range of $\delta = 0$–0.5. Since the oxidation states of the often multivalent cations in these materials are intimately related to oxygen composition in the crystal lattice and, in turn, the cation valence states control the catalytic properties and ionic conduction, the ability to control the oxygen vacancies in $ABO_{3-\delta}$ perovskite films will enhance the likelihood of their application in energy conversion, production and storage [2–10].

Experimental techniques used for monitoring oxygen contents in bulk oxides, e.g. thermogravimetric analysis [11, 12], are hardly applicable for ABO_3 type perovskite thin film systems for practical reasons. Very often few monolayers of one type of ABO_3 system are grown on a thick $A'B'O_3$ system of different chemistry and the propensity of oxygen loss of each system could markedly differ. Recently, Xie *et al* studied reversible oxygen loss in $La_{1-x}Sr_xFeO_{3-\delta}$ (LSFO) films through a combination of transport measurements, ellipsometry and x-ray diffraction studies [13]. Their results reveal that reversible control of oxygen content through reduction and oxidation of the film at temperatures as low as 200 °C can induce significant changes in electrical resistivity, optical absorption and lattice size. Similar behavior has also been recently reported for $SrCoO_{3-\delta}$ films [14].

While XRD provides average crystal structure, and with transport and optical measurements, phenomenological understanding of cation oxidation states in ABO_3 type perovskites, Raman scattering spectroscopy is effective for probing the onset of a phase transition with local correlation lengths as few as several unit cells. Raman scattering is non-destructive in identifying structural and electronic phases in solids, thin films, and nanostructured semiconductor and oxide materials, since scattering by phonons and electronic degrees

 © 2015 IOP Publishing Ltd Printed in the UK

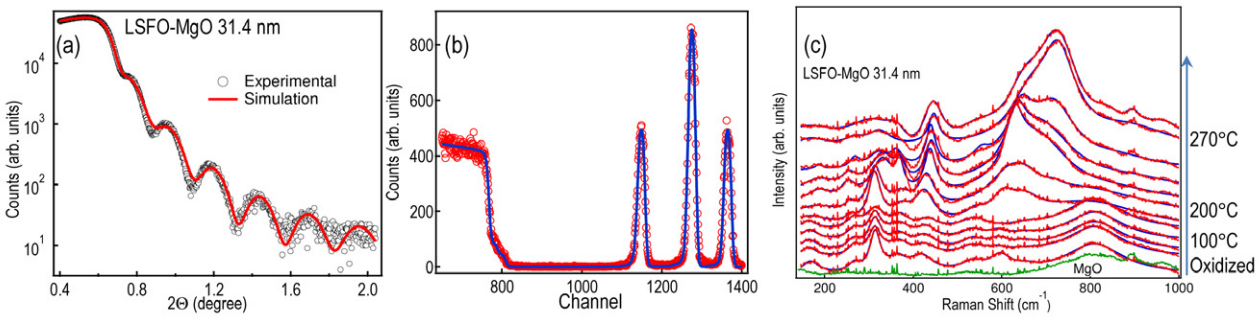

Figure 1. (*a*) X-ray reflectivity results, indicating a film thickness of 31.4 nm. (*b*) Measured Rutherford backscattering spectroscopy and fitting of film deposited on MgO(0 0 1) crystal as described in the text, indicating stoichiometry as $La_{0.2}Sr_{0.8}FeO_3$. (*c*) Evolution of Raman scattering spectra measured at 300 K in air in an MgO(0 0 1) crystal (cyan) and in the 31.4 nm-thick $La_{0.2}Sr_{0.8}FeO_3$ (LSFO) film deposited on MgO immediately after oxidation and after air annealing at different temperture as denoted next to the figure.

of freedom together provide unique signatures of atomic, polar and electronic ordering. Previous studies have provided critical information about impurities, internal stress, crystal symmetry, and polar order in various complex oxide films [15–20].

Studying structural and electronic phases through Raman spectroscopy using visible laser line excitation in thin films of wide band gap ABO_3 perovskites is challenging due to weak absorption and to contributions from typical perovskite substrates used. Accordingly, we selected $La_{1-x}Sr_xFeO_{3-\delta}$ (LSFO) on MgO(0 0 1) due to weak Raman response in the energy of interest (200–700 cm^{-1}) for LSFO and weak Raman scattering from MgO compared to perovskite substrates.

Here, we report on evolution of Raman scattering at different stages of annealing in air, and oxygen loss induced symmetry-lowering of a complex oxide perovskite thin film resulting in the activation of normally IR-active modes. Coupled with carrier transport collected from this system under identical conditions indicating a rapid increase in the resistivity, these results provide semiquantitative correlation between the loss of oxygen and mode hardening, and significantly, suggest a topotatic transformation of the crystal structure from that of the rhombohedral ABO_3 perovskites to that of Brownmillerite-like structure consisting of octahedrally and tetrahedrally coordinated Fe atoms.

2. Experimental details

The (La,Sr)FeO_3 films were deposited onto single crystal MgO(0 0 1) using molecular beam epitaxy, in which the cations were evaporated from effusion cells under a 5%/95% mixture of O_3/O_2 as the oxidizing environment [21]. Growth temperatures and pressures were typically 575 °C to 650 °C and (2–8) × 10^{-6} Torr, respectively. Following growth, the (La,Sr)$FeO_{3-\delta}$ films were annealed in oxygen for 4 h. at 650 °C and then in a tube furnace under flowing O_3/O_2 (5%/95%) at 200 °C for 30 min [22]. This same procedure was used to re-oxidize films after they had been reduced. X-ray reflectivity (XRR) measurements were performed using a Rigaku SmartLab instrument. The thickness of the film was determined by quantitative analysis of XRR data (fitting using GenX software) to be 31.4 nm (figure 1(*a*)). Rutherford backscattering spectrometry (RBS), carried out with 2 MeV He ions with a 0° incident angle and a 163° scattering angle, was used to determine the $La_{0.2}Sr_{0.8}FeO_3$ stoichiometry (figure 1(*b*)). The cation composition was obtained by minimizing the difference between the measured and simulated spectra calculated using the SIMNRA software package [23]. Film reduction was carried out by heating films in the ambient on a hot plate; the hot plate temperature was verified by a thermocouple to be within ±3 °C of the set point temperature.

Raman scattering spectra were collected at 300 K in air from the film immediately after the film deposition and after O_3/O_2 annealing, and after each reduction step. Raman scattering spectra were excited using the linearly polarized output of a solid state laser (532 nm) with 3.75 mW of power in a spot diameter of 0.5 μm at the sample, and were dispersed and detected using a single-axis monochromator equipped with a charge-coupled detector array (Horiba XploRA, Edison NJ). All Raman spectra were collected unpolarized and in the backscattering geometry. Electrical resistivity of the films was measured in a Physical Properties Measurement System (Quantum Design, San Diego, CA) using external electronics to source current (Keithley Model 6220) and measure voltage (Keithley Model 2182A). Film resistivity was measured in a linear four point geometry with silver paint used to make contacts. After each 300 K resistivity measurement, the contacts were removed using acetone and IPA in ultrasonicator.

3. Results and discussion

The 300 K Raman spectra from a bare MgO(0 0 1) substrate and from the 31.4 nm-thick LSFO film on MgO(0 0 1) following different stages of annealing in air are shown in figure 1. LSFO films are found to exhibit gradual increases in 300 K resistivity when heated in air at temperatures as low as 100 °C, increases that become more pronounced after films are heated to 200 °C and beyond [13]. MgO has the rocksalt structure and is thus expected to show no first-order Raman scattering [16, 24]. In some studies second order Raman features were seen for specific polarizations and crystal orientations. In our study, two broad features centered around 532 cm^{-1} and 808 cm^{-1} are observed, which are close to the features seen in previous studies [24]. No significant changes to these features were seen

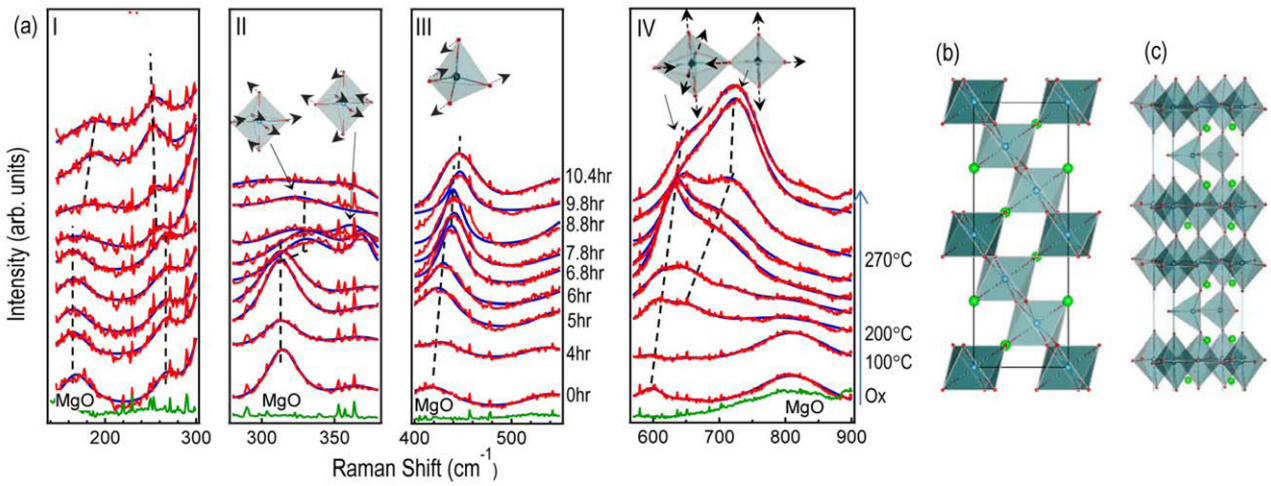

Figure 2. (*a*) Selected range of the Raman scattering spectra measured at 300 K in air in an MgO(0 0 1) crystal (cyan) and in the 31.4 nm-thick $La_{0.2}Sr_{0.8}FeO_3$ (LSFO) film deposited on MgO immediately after oxidation and after each timed air annealing step as denoted in the figure next to panels III and IV. For clarity the spectra are offset vertically. While the MgO substrate shows two broad, weak bands centered on 533 cm^{-1} and 800 cm^{-1}, the spectrum of thin-film LSFO possesses several peaks that evolve with annealing time and temperature. Also plotted are Lorentzian-fitted lineshapes of the LSFO Raman spectra, including a background. Selected normal mode vibrations patters contributing to each band are illustrated above the spectra. The structures of the rhombohedral ABO_3 perovskite and that to which we propose it transforms, a Brownmillerite-like structure consisting of octahedrally and tetrahedrally coordinated Fe, are shown in (*b*) and (*c*), respectively. The narrow lines seen in the spectra, predominantly between 200 and 700 cm^{-1}, are a common feature when multichannel CCD detectors are used in Raman spectroscopy, especially when signal is weak and accumulation times are long, as in this case. We can't rule out the possibility of cosmic ray origin of these lines.

when the substrate was heated under the same conditions as the sample containing the LSFO film. Based on comparison of the spectra collected from the LSFO film on an MgO substrate with the bare substrate, we assign the band at 808 cm^{-1} (figure 2(*a*)-IV) to MgO; this will not be discussed further. We divide the remaining spectrum in four regions of interest (I–IV) and discuss these in detail below.

To facilitate discussion of the Raman scattering measurements, we provide a brief summary of the LSFO crystal structure and its possible transition into an oxygen-deficient form. LSFO is a typical mixed cation ABO_3 type perovskite that has a rhombohedral structure in the ambient conditions and belongs to the space group $R\bar{3}c$ with two formula units per unit cell (figure 2(*b*)) [25]. Previous experiments have shown the strong propensity of LSFO for oxygen loss, even in the ambient. The loss of oxygen can be accelerated through heating LSFO in air at temperatures at low as 200 °C, as was done in our experiments and elsewhere [13]. As such we consider the possibility of a topotactic transition of the LSFO film. A topotactic transition is a structural phase change in a crystal lattice mediated by loss or gain of elements, with the final structure retaining one or more of the crystallographic framework of the parent phase. We propose here a topotactic phase transformation of our LSFO film from simple perovskite structure to a defect perovskite with *ca.* 13% vacancies on the anion positions with Brownmillerite-like structure. For example, the reduced form of $La_{1/3}Sr_{2/3}FeO_3$ is $LaSr_2Fe_3O_8$ consisting of double layers of perovskite-type corner connected BO_6 octahedra and single chains of BO_4 tetrahedra (figure 2(*c*)) [26].

Normal mode enumeration shows that perovskites with the rhombohedral crystal structure (e.g. LSFO) has 27 optical modes and are classified as $A_{1g}(R) + 4E_g(R) + 3A_{2u}(IR) + 5E_u(IR) + 2A_{1u} + 3A_{2g}$ [25, 27, 28]. Of the five Raman-active modes, four ($3E_g + 1A_{1g}$) involve vibrations associated with the FeO_6 octahedra while the remaining E_g mode involves vibration of the La/Sr ions [27, 28]. On the contrary, perovskites with Brownmillerite-like structure with $A_3B_3O_8$ chemistry (e.g. $Ca_2LaFe_3O_8$ and $LaSr_2Fe_3O_8$, space group *Pmma*) have 60 possible Raman-active vibrational modes: $17A_g + 12A_{1g} + 15B_{2g} + 16B_{3g}$ [26, 29].

We are unaware of any reports of lattice dynamics calculations (LDC) performed on LSFO, perhaps due to the computational cost of constructing relatively large unit cells to represent the composition in this mixed cation system. Accordingly, the assignment of the Raman modes observed in our LSFO films is guided by LDC of Abrashev *et al* for the rhombohedral r-$LaMnO_3$, by experimentally observed Raman modes in bulk LSFO, and by experimentally observed Raman features by Lazic *et al* [28–30].

3.1. Region IV, 590–800 cm^{-1}: the stretching modes

A broad Raman band in the vicinity of 650 cm^{-1} has been seen frequently in ABO_3 perovskite Raman spectra and has lately been the topic of considerable discussion (see, e.g. [27] and [29]). In most studies of rhombohedral ABO_3 perovskites this feature is usually found to be close to one of the calculated Raman active E_g or IR active A_{2u} or E_u modes. However, in most cases this band doesn't follow the selection rule or the expected trends with cation substitution or temperature increase/decrease [28, 30].

In rhombohedral ABO_3 systems the appearance and evolution of this mode instead follow what would be expected

from dynamic Jahn–Teller (JT) effects [31]. The rhombohedral system is, however, incompatible with JT interactions due to its six equal *B*–O bonds, and JT vibrations can only be activated with compatible charge configurations (e.g. d^4) on the *B* atoms. Nevertheless, in systems with d^3 or d^5 configurations localized electrons and local symmetry breaking can result in incoherent and dynamic JT vibrations in rhombohedral ABO_3 type perovskite systems [27].

LSFO is a perfect example of such interplay between the crystal lattice and the orbital distribution of the electrons. Generally in ABO_3 perovskites the O atoms are in the charge state of O^{2-}. With this scheme the charge states on the octahedra in LSFO should be $Fe^{3.8+}3d^{4.2}$; this state is considered nominally Fe^{4+} ($3d^4$). However, photoemission studies have confirmed that the electronic structure of Fe^{4+} is unconventional: the charge transfer energy Δ, the energy required to transfer an electron from the oxygen *p* to Fe 3*d* level, is negative and the ground state of the formal Fe^{4+} ('d^4') state is in fact dominated by the d^5L configuration, where *L* denotes a hole in the oxygen 2*p* band [32]. This scheme has been used to explain the fact that, unlike rhombohedral manganites with J–T compatible electronic structures, the LSFO system exhibits very weak J–T type Raman bands.

As shown in panel IV of figure 2(*a*) our LSFO films exhibit a weak band centered on 597 cm^{-1} in the oxidized sample and this continues to monotonically blue shift as the sample is heated, consistent with the previous reports. We consider this band to be a J–T like mode, being activated by the breaking of symmetry of the rhombohedral structure due to oxygen deficiency. However, after the sample is heated to 200 °C the spectra change: the peak associated with this weak J–T type Raman band undergoes a significant blue shift (panel IV within figures 2(*a*) and 3) and the intensity also increases. In addition, a higher energy shoulder appears after the first 200 °C annealing, gradually developing into a full band when the sample is heated at 270 °C (panel IV within figures 2(*a*) and 3). These results indicate clearly that the loss of oxygen is directly related to the activation and strong increase of intensity and blue shifts of these two modes.

Removing oxygen from LSFO is tantamount to removing ligand holes (*L*). For example, the removal of oxygen in our LSFO film, which is d^5L (nominally, d^4), results in more of the sample having the Fe^{3+} (d^5) state. Thus, once the ligand holes are removed, the system becomes populated with higher percent of Fe^{3+} compared to Fe^{4+}, which should result in less tendency of the system to exhibit dynamic J–T vibrations. The opposite is, however, seen in our experiments (figure 2(*a*)). This apparent contradiction between the oxygen vacancy-induced transition of the LSFO crystal to one highly populated with Fe^{3+}, as shown by higher resistivity [13], and the *higher* intensity of the J–T type bands can be can be reconciled, however, if one considers a change of crystal structure of LSFO with loss of oxygen. We propose that as oxygen atoms are removed, the system undergoes a transition from the rhombohedral structure—incompatible with J–T vibrations—to the orthorhombic structure which is compatible with such distortions. The blue shift of this peak could be a result of stiffening of the Fe–O bonds due to loss of oxygen from the lattice.

This assertion is further strengthened by the fact that with a 13% loss of oxygen an ABO_3 perovskite can, in principle, topotactically transition into a oxygen deficient Brownmillerite-like structure with $A_3B_3O_8$ chemistry. Examples of similar crystals include $Ca_2LaFe_3O_8$ and $LaSr_2Fe_3O_8$. The point group of the crystal symmetry of these materials is orthorhombic and the space groups of *Pmma*, *Pm*2*a* and *P*2$_1$*ma* have been observed [26, 29]. Structurally, the Brownmillerite-like structure with $A_3B_3O_8$ chemistry is composed of double layers of perovskite-type corner connected BO_6 octahedra and single chains of BO_4 tetrahedra (figure 2(*c*)) [26].

Our assertion of the topotactic transition of LSFO with oxygen loss is further supported by the second significant observation: the emergence, strengthening and blue shift of a band to the higher energy side of the J–T like modes (panel IV within figures 2(*a*) and 3). A recent Raman study of the Brownmillerite crystal $Ca_2Al_2O_5$ found the stretching modes of the AlO_6 octahedra and the AlO_4 tetrahedra to be centered on 739 cm^{-1} and 772 cm^{-1}, respectively. These results are well corroborated with the shorter interatomic distance within the tetrahedral units as determined by x-ray diffraction [29]. Various chain silicates like $NaYSi_2O_6$, $Na_6Si_8O_{19}$, and $K_4SrSi_3O_9$ show very similar spectra with intense bands around 900–1100 cm^{-1}, related to SiO_4 tetrahedral stretching [33]. The higher energy vibrations in the silicate crystals can be explained by the stronger bonding and shorter interatomic distances of Si–O compared with Al–O.

We thus assign the mode centered initially on 650 cm^{-1} in our LSFO films to emanate from the stretching modes of FeO_4 tetrahedra from regions of the crystal that have transformed into Brownmillerite-like structure having $La_{0.6}Sr_{2.4}Fe_3O_8$ chemistry. The increase in intensity could be due to the increased volume of crystal inhabited by FeO_4 as more and more of the oxygen is lost from the sample.

3.2. Region III: the bending mode of the FeO_4 tetrahedra

As shown in figure 2(*a*)-III a Raman band in the vicinity of 417 cm^{-1} is present in the spectrum of the oxidized sample and monotonically blue shifts as the sample is heated. When the sample is annealed at 200 °C, this band gradually grains strength and blue shifts further. Evolution of this peak qualitatively coincides with that of the peak assigned to the stretching mode of the FeO_4 tetrahedra. The bending mode frequency of the AlO_4 tetrahedra in a recent Raman study of the Brownmillerite crystal $Ca_2Al_2O_5$ was found to be at 476 cm^{-1}, and the same mode of the SiO_4 tetrahedra in $K_4SrSi_3O_9$ crystal was found out to be in the 450–700 cm^{-1} range [29, 33]. We therefore assign this peak to the bending mode of the FeO_4 tetrahedra in our LSFO film. The significantly lower value seen in our sample could be as result of weaker interatomic forces in the FeO_4 tetrahedra compared to that in AlO_4 tetrahedra and SiO_4 tetrahedra, possibly due to weaker covalency in the Fe–O bonds.

3.3. Region II: the IR modes modes of LSFO

The Raman bands centered on 313 cm^{-1} and 365 cm^{-1} in the oxidized sample (figure 2(*a*)-II) have qualitatively different

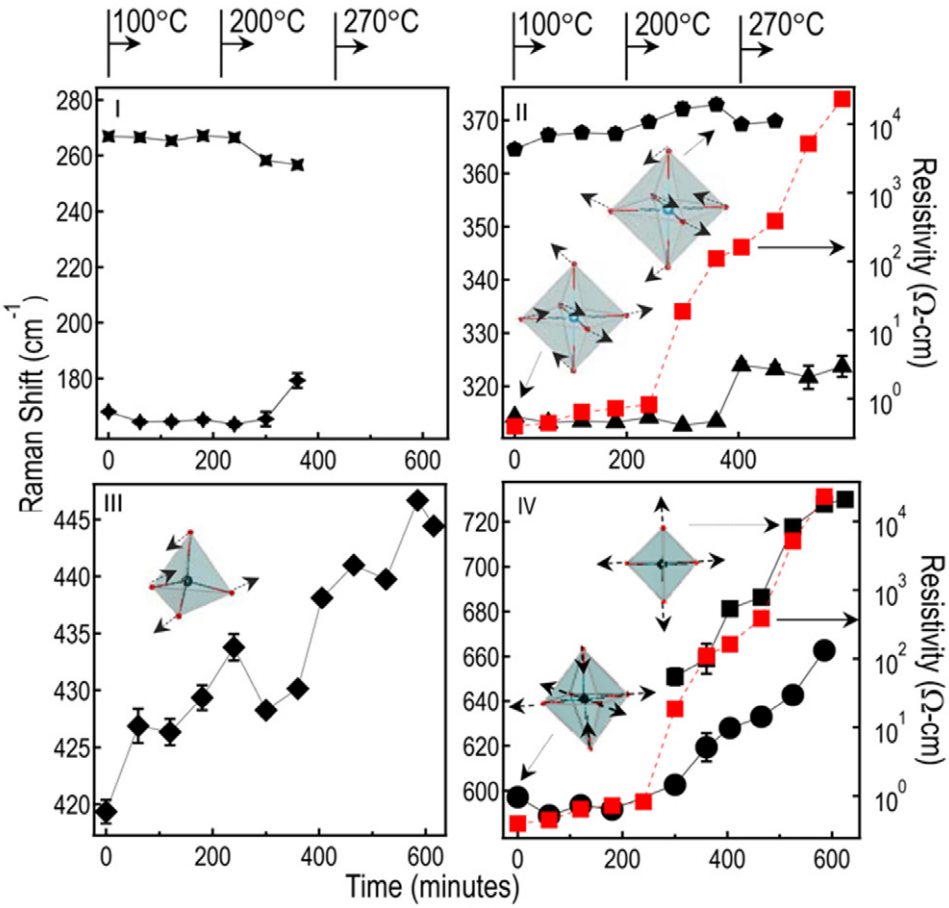

Figure 3. Fitted peak positions of the major 300 K Raman bands are displayed as a function of annealing temperature and time. The changes of temperature noted above in panels (*a*) and (*b*) also apply for the data in panels (*c*) and (*d*). The normal mode lattice displacements contributing to Raman bands are illustrated in each plot. Also plotted in (*b*) and (*d*) (right ordinate) is the evolution of the resistivity following each air annealing step indicating strong correlation with changes in J–T mode response and activation of a stretching mode associated with the Brownmillerite-like structure (*d*).

behavior to those in region III. Specifically, the intensities of these peaks, while present in the oxygen-rich sample, increase with oxygen loss at 200 °C, but the peaks essentially disappear when the crystal structure changes after heating at 270 °C. The evolutions of these peaks qualitatively coincide with that of the peak assigned to the stretching mode of the FeO_6 octahedra in region IV. Thus, we attribute these peaks to normal vibrations of the oxidized rhombohedral LSFO.

The assignment of these modes follows analysis of experimentally observed Raman modes in bulk LSFO by Ghosh *et al* [30] and lattice dynamics calculations (LDC) performed by Abrashev *et al* for the rhombohedral r-$LaMnO_3$ [28]. The energies of these two modes, while seen experimentally in bulk LSFO, are not similar to any of the Raman active modes calculated for r-$LaMnO_3$. Rather, they are close to the calculated IR modes of r-$LaMnO_3$. Thus, we assign the bands centered on 313 cm^{-1} and 365 cm^{-1} to the IR-active modes of A_{2u} (TO) and E_u (TO) symmetry, respectively. As for their LO counterparts, we believe contribution from these modes result in the weak bands centered on 417 cm^{-1} and 538 cm^{-1} in the oxidized sample, as seen in figure 2.

To discuss the assignment and dynamics of these modes it is helpful to point out briefly the mode dissociation from the original cubic structure $Pm3m$ to rhombohedral $R\bar{3}c$. The original zone center T_{1u} mode of the cubic system dissociates into A_{2u} and E_u modes in the rhombohedral system. Each of the polar A_{2u} and E_u mode further splits into transverse (TO) and longitudinal (LO) modes due to the long-range electric field. While the A_{2u}—E_u splitting of the parent T_{1u} depends on the magnitude of rhombohedral distortion (less distortion—less splitting), the LO/TO splitting of the individual polar modes depends on the magnitude of the long range electric field. Our assignments are qualitatively based on the above effects.

While small rhombohedral distortions in LSFO (compared to other $R\bar{3}c$ systems) are expected to result in small force constant anisotropies in LSFO, dynamic loss of oxygen is expected to produce large electric fields in the system. We believe, in our sample the former results in small splittings in the neighboring A_{2u}(TO)–E_u(TO) modes while the latter results in strong TO/LO splittings in the same symmetry mode. Similar results have been seen in other ABO_3 perovskite systems and wurtzite type structures [28, 34].

The change of crystal structure with loss of oxygen from the lattice makes it difficult to analyze the evolution of the peak positions. However, we still make an attempt to relate oxygen loss with the shift of frequency of the mode centered

at 313 cm^{-1} in the nominally stoichiometric sample that shifts to 325 cm^{-1} when the sample is heated at 270 °C, as shown in figures 2(*a*)-II and 3(*b*). The increase in frequency can be semiquantitatively explained by the loss of oxygen from the LSFO lattice. The frequency of a normal mode of symmetry Γ is inversely proportional to the square root reduced mass M_Γ of the atoms participating in the mode: $\frac{1}{M_\Gamma} = \sum_i \frac{1}{M_i}$. Assuming all the six oxygens in the octahedra participate in the bending mode vibrations, the frequency shift from 311 cm^{-1} to 325 cm^{-1} would entail a 0.32 O vacancies per formula unit. This is remarkably close to the 0.33 O vacancies per formula units in the reduced LSFO ($La_{0.6}Sr_{2.4}Fe_3O_8$ is $La_{0.2}Sr_{0.8}FeO_{2.67}$).

3.4. Region I: A_{1g} modes of the static octahedral rotation and E_g mode of A cation displacement

The Raman peak centered on 266 cm^{-1} (figures 2(*a*)-I and 3(*a*)) in the oxidized sample is assigned to the rotation of the FeO_6 octahedra of A_{1g} symmetry, following previous results [28, 30]. The vibrational pattern of the Raman feature of A_{1g} symmetry in $R\bar{3}c$ crystal structures is correlated with rhombohedral distortion, which is the static rotational displacement of the oxygen octahedra around the hexagonal $[0\,0\,1]_h$ direction.

The frequency of this mode is generally found to directly correlate to the magnitude of the rhombohedral distortion. For example, in $RAlO_3$ (R = La, Pr, Nd) the A_{1g} mode frequency (at room temperature) shifts by a factor or 2 (from 122 cm^{-1} for R = La to 241 cm^{-1} for R = Nd) due to the increase of the rhombohedral distortion upon decrease of the radius of the R ion [35]. In a related study, the A_{1g} mode frequency was found to be 132 cm^{-1} in $LaAlO_3$, which increased to 249 cm^{-1} in $LaMnO_3$, due to increase in rhombohedral distortion in going from the former system to the latter.

Our assignment of the 266 cm^{-1} feature to A_{1g} mode in the rhombohedral LSFO system closely correlates the above line of reasoning. Since the atomic radius of Mn is very close to that of Fe, it's reasonable to assume that the A_{1g} mode frequency in $LaFeO_3$ will be close to that of $LaMnO_3$, namely 249 cm^{-1}. Hence we consider the frequency of the static octahedral rotation of A_{1g} symmetry in our LSFO sample of 266 cm^{-1} to be reasonable.

Annealing the LSFO film at temperatures up to 200 °C does not produce any noticeable change in the frequency and the intensity of this feature: as long as the crystal structure doesn't change, on the average the overall rotation of the octahedra does not depend critically on the oxygen content. Annealing at 270°C however, results in quenching of this mode as seen from figure 2(*a*), perhaps due to change in crystal structure.

Finally, the Raman feature, centered on 168 cm^{-1} (figures 2(*a*)-I and 3(*a*)) in the oxidized sample is assigned to the motion of the La and/or Sr atoms, following the lattice dynamics calculations of r-$LaMnO_3$ [28]. As shown in figure 2(*a*)-I the mode is unchanged as long as the sample is heated at temperature of 200 °C or less. Beyond that the mode is quenched due, again, to the change in crystal structure and the *A* cation experiencing different surroundings.

3.5. Comparison of evolution of Raman scattering energies with resistivity in LSFO thin films

The measured resistivity in the identical LSFO film, which increases modestly at heating temperature of 100 °C, increases by almost three orders of magnitude after heating in air for three hours at 200 °C and by another two orders of magnitude after subsequent heating in air for two hours at 270 °C. To compare the loss of oxygen from the crystal lattice with the evolution of the vibrational modes, we plot in figure 3 measured changes in resistivity along with selected modes (IR octahedral bending modes (*b*) and the J–T like modes (*d*)). A clear and almost one-to-one correlation is seen between temperatures at which mode energies (left axes) and the resistivity (right axis) change for the J–T like modes, supporting our assertion of an oxygen vacancy mediated transition of the crystal structure. The orders of magnitude increase in resistivity upon heating of the samples in the ambient is due to the escape of oxygen atoms from the lattice and subsequent trapping of charge carrier polarons at the oxygen vacancies [13]. In this film, the oxygen loss reduces the iron valence from a nominal 3.8^+ toward the more stable 3^+. Previous work on both $La_{1-x}Sr_xFeO_3$ and $SrFeO_{3-\delta}$ has established a trend toward more insulating behavior as the nominal Fe valence is reduced from 4^+ to 3^+ [7, 36, 37]. Similar increases in resistivity with oxygen loss are also observed in other perovskite films such as $SrCoO_{3-\delta}$ and $SrCrO_{3-\delta}$ [38, 39]. These significant changes in resistivity after annealing at 200 °C and 270 °C correspond well with observed changes in Raman, particularly modes in (*d*).

The entire process of introducing oxygen vacancies via annealing in air, and ultimately a phase transformation, as observed by Raman scattering, is reversible and reproducible. Following Raman scattering and carrier transport measurements the LSFO film was returned to its as-grown stoichiometric state by annealing in a 5%/95% mixture of O_3/O_2 environment at a temperature of 200 °C for 30 min. The process of heating to gradually reduce the sample at the above mentioned temperatures, and collection of Raman scattering and carrier transport measurements at 300 K was carried out again on this sample and nearly identical results were reproduced after annealing at each temperature and time.

4. Conclusion

Measuring and controlling the loss of oxygen is a critical challenge in perovskite film synthesis and complex oxide electronics. Evolution of Raman scattering by phonons in LSFO as a model system at different stages of annealing in air to alter oxygen content and cation oxidation state can now be considered a sensitive probe of oxygen content in complex oxide perovskite thin films. Significantly, these results also point to observability by Raman scattering of a reversible, reduced-anneal and oxidative recovery topotactic phase transition in complex oxide perovskite thin films.

Acknowledgments

The authors gratefully acknowledge the ONR (N00014-11-1-0664) for support of this work, and the Drexel

Centralized Research Facilities for access to and support of instrumentation. MDS acknowledges support from the Department of Education (GAANN-RETAIN, Award No. P200A100117). We thank L Wielunski for RBS measurements at the Laboratory for Surface Modification at Rutgers University.

References

[1] Dagotto E 2005 *Science* **309** 257
[2] Grinberg I *et al* 2013 *Nature* **503** 509
[3] Jeong J, Aetukuri N, Graf T, Schladt T D, Samant M G and Parkin S S P 2013 *Science* **339** 1402
[4] Mitchell J F, Argyriou D N, Potter C D, Hinks D G, Jorgensen J D and Bader S D 1996 *Phys. Rev.* B **54** 6172
[5] Sanchez R D, Causa M T, Caneiro A, Butera A, Vallet-Regi M, Sayagues M J, Gonzalez-Calbet J, Garcia-Sanz F and Rivas J 1996 *Phys. Rev.* B **54** 16574
[6] Gayathri N, Raychaudhuri A K, Xu X Q, Peng J L and Greene R L 1998 *J. Phys.: Condens. Matter* **10** 1323
[7] Adler P, Lebon A, Damljanović V, Ulrich C, Bernhard C, Boris A V, Maljuk A, Lin C T and Keimer B 2006 *Phys. Rev.* B **73** 094451
[8] Suescun L, Chmaissem O, Mais J, Dabrowski B and Jorgensen J D 2007 *J. Solid State Chem.* **180** 1698
[9] Kalinin S V, Borisevich A and Fong D 2012 *ACS Nano* **6** 10423
[10] Kalinin S V and Spaldin N A 2013 *Science* **341** 858
[11] Machida M, Kawamura K, Ito K and Ikeue K 2005 *Chem. Mater.* **17** 1487
[12] Rsnen S, Motohashi T, Yamauchi H and Karppinen M 2010 *J. Solid State Chem.* **183** 692
[13] Xie Y, Scafetta M D, Sichel-Tissot R J, Moon E J, Devlin R C, Wu H, Krick A L and May S J 2014 *Adv. Mater.* **26** 1434
[14] Choi W S, Jeen H, Lee J H, Seo S S A, Cooper V R, Rabe K M and Lee H N 2013 *Phys. Rev. Lett.* **111** 097401
[15] Spanier J E, Levy M, Herman I P, Osgood R M and Bahalla A S 2001 *Appl. Phys. Lett.* **79** 1510
[16] Yuzyuk Y I, Alyoshin V A, Zakharchenko I N, Sviridov E V, Almeida A and Chaves M R 2002 *Phys. Rev.* B **65** 134107
[17] Dore P, Postorino P, Sacchetti A, Baldini M, Giambelluca R, Angeloni M and Balestrino G 2005 *Eur. Phys. J.* B **48** 255
[18] Tenne D A *et al* 2006 *Science* **313** 1614
[19] Kreisel J, Weber M C, Dix N, Snchez F, Thomas P A and Fontcuberta J 2012 *Adv. Funct. Mater.* **22** 5044
[20] Iliev M N, Guo H and Gupta A 2007 *Appl. Phys. Lett.* **90** 151914
[21] Scafetta M D, Xie Y J, Torres M, Spanier J E and May S J 2013 *Appl. Phys. Lett.* **102** 081904
[22] Yamada H, Kawasaki M and Tokura Y 2002 *Appl. Phys. Lett.* **80** 622–4
[23] Mayer M 1997 *SIMNRA Users Guide* (*Report IPP 9/113, Max-Planck-Institut fur Plasmaphysik*) (Germany: Graching)
[24] Manson N B, Von der Ohe W and Chodos S L 1971 *Phys. Rev.* B **3** 1968
[25] Islam M A, Rondinelli J M and Spanier J E 2013 *J. Phys.: Condens. Matter* **25** 175902
[26] Battle P, Gibb T and Lightfoot P 1990 *J. Solid State Chem.* **84** 237
[27] Iliev M N and Abrashev M V 2001 *J. Raman Spectrosc.* **32** 805
[28] Abrashev M V, Litvinchuk A P, Iliev M N, Meng R L, Popov V N, Ivanov V G, Chakalov R A and Thomsen C 1999 *Phys. Rev.* B **59** 4146
[29] Lazic B, Krger H, Kahlenberg V, Konzett J and Kaindl R 2008 *Acta Crystallogr.* B **64** 417
[30] Ghosh S, Kamaraju N, Seto M, Fujimori A, Takeda Y, Ishiwata S, Kawasaki S, Azuma M, Takano M and Sood A K 2005 *Phys. Rev.* B **71** 245110
[31] Radaelli P G, Marezio M, Hwang H Y, Cheong S W and Batlogg B 1996 *Phys. Rev.* B **54** 8992
[32] Bocquet A E, Fujimori A, Mizokawa T, Saitoh T, Namatame H, Suga S, Kimizuka N, Takeda Y and Takano M 1992 *Phys. Rev.* B **45** 1561
[33] Kahlenberg V, Kaindl R and Sartory B 2007 *Solid State Sci.* **9** 65
[34] Loudon R 1964 *Adv. Phys.* **13** 423
[35] Wen-Chen Z 1995 *J. Phys.: Condens. Matter* **7** 4499
[36] Maeder T and Bednorz J G 1999 *J. Eur. Ceram. Soc.* **19** 1507
[37] Xie Y J, Scafetta M D, Moon E J, Krick A L, Sichel-Tissot R J and May S J 2014 *Appl. Phys. Lett.* **105** 062110
[38] Jeen H, Choi W S, Freeland J W, Ohta H, Jung C U and Lee H N 2013 *Adv. Mater.* **25** 3651
[39] Zhang P V, Sushko K H L, Colby Y, Du R, Bowden M E and Chambers S A 2014 *Nat. Commun.* **5** 5669